PHYSICAL REVIEW C VOLUME 27, NUMBER 3 MARCH 1983

Spin orbit effects in quasifree knockout reactions

N. S. Chant and P. G. Roos
Department of Physics and Astronomy, University of Maryland, College Park, Maryland 20742
(Received 27 September 1982)

An efficient calculational method for distorted wave impulse approximation analyses of quasifree knockout reactions is described. Since the usual Racah algebra is eliminated, it is straightforward to include spin-orbit distortions. Results are presented for 150 MeV $(p,2p)$ and (p,pn) reactions. In some cases the effects of the spin-orbit terms are large.

[NUCLEAR REACTIONS Effect of spin-orbit distortions in distorted wave impulse approximation calculation for $(p,2p)$ and (p,pn) reactions.]

I. INTRODUCTION

Quasifree knockout reactions such as $(p,2p)$ or $(p,p\alpha)$ have been studied in recent years in order to obtain information on the nucleon or nucleon cluster parentage of nuclei.[1-6] Such studies complement the analogous transfer reactions which are usually restricted to higher momentum components. An additional feature of the knockout reaction studies is the possibility, at least in principle, of studying the projectile-nucleon or projectile-cluster interaction off the energy shell. Regrettably, little work has been reported in this connection. Partially this reflects experimental difficulties and partially it is a consequence of limitations of current theoretical descriptions of the reaction.

Most current theoretical analyses of knockout reaction data employ a distorted wave impulse approximation (DWIA) calculation.[7,8] Usually a so-called "factorization" approximation is introduced so that the projectile-struck particle elastic scattering *cross section* enters as a multiplicative factor. This feature is a serious drawback to studies of off-shell effects since, more properly, the corresponding two-body t matrix should be evaluated in the nuclear medium.

For present purposes the factorized form for the DWIA cross section can be regarded as arising from two approximations. Firstly, the transition operator occurring in the distorted wave integral is replaced by a two-body t matrix evaluated at the asymptotic kinematics. Secondly, spin-orbit terms in the optical potentials used to generate the projectile and emitted particle scattering wave functions are omitted. As a result, simplification of the spin summations leads to the appearance of the two-body cross section as a multiplicative factor. It is the elimination of the latter approximation which is the subject of the present paper. Thus, the calculations we will present, including spin-orbit effects, utilize factorization of the amplitude into DWIA and fully spin dependent two-body terms, but no simplification of the spin summations is possible.

Approximate methods which attempt to correct for the factorization approximation have been described,[9-11] and one calculation has been reported.[11] In addition, for $(p,2p)$, some exact calculations for a local pseudopotential have been reported[12] and extended using a momentum representation.[13] Unfortunately, in all cases, the spin structure of the two-body p-p transition operator is much simplified and spin-orbit distortions are omitted.

Clearly, detailed studies of off-shell effects must await the elimination of both the limitations of current calculations. Nevertheless, the inclusion of spin dependence in the optical potentials is of interest in view of recent $(p,2p)$ studies employing polarized incident beams as well as proposals to study cluster knockout reactions induced by polarized protons.

In a previous publication[14] we presented our first calculations of the effects of including spin-orbit distortions in the DWIA theory of $(p,2p)$ reactions. In order to carry out these calculations in an acceptable amount of computing time, it was necessary to introduce an unconventional numerical technique which eliminates the need for Racah algebra. In the present paper we first describe our new method of calculation. This is to be found in Sec. II, in which the basis of the method is given, after which the theory is recast in a form suitable for calculation. Second, in Secs. III and IV, we present and discuss additional results for the effect of spin-orbit terms in $(p,2p)$ and (p,pn) reactions.

II. METHOD OF CALCULATION

A. Basis of the method

Let us consider a quasifree knockout reaction $A(a,cd)B$ where $A=B+b$. As is well known,[7,8] a factorized DWIA calculation for such a reaction involves the evaluation of an amplitude

$$T^{L\Lambda}=(2L+1)^{-(1/2)}\int \chi_c^{(-)*}(\vec{r})\chi_d^{(-)*}(\vec{r})\phi_{L\Lambda}(\vec{r})\chi_a^{(+)}(\gamma\vec{r})d\vec{r}\,, \tag{1}$$

where $\gamma=B/A$, the $\chi^{(\pm)}$ are distorted waves, and $\phi_{L\Lambda}$ is the spatial part of the bound state wave function of particle (or cluster) b. The quantities L and Λ are, respectively, the orbital angular momentum carried by b and its projection.

If spin-orbit terms are neglected, the use of conventional techniques of Racah algebra yields the following expression:

$$T^{L\Lambda}\propto \sum_{\substack{l_a l_c l_d \\ kq}} i^{l_a+L-l_c-l_d}\frac{(2l_a+1)(2l_c+1)(2l_d+1)}{(2k+1)} \times(l_d\lambda_d L\Lambda\,|\,kq)(l_d 0L0\,|\,k0)(l_a 0l_c q\,|\,kq)(l_a 0l_c 0\,|\,k0)I^L_{l_a l_c l_d}d^{l_c}_{q0}(\theta_c)d^{l_d}_{\lambda_d 0}(\theta_d)e^{-i\lambda_b\phi_b}\,, \tag{2}$$

where $(l_1\lambda_1 l_2\lambda_2\,|\,l_3\lambda_3)$ is a Glebsch-Gordan coefficient, $d^l_{mn}(\theta)$ is a reduced rotation matrix element, and $I^L_{l_a l_c l_d}$ is a radial integral. Details can be found elsewhere.[7] For the present, we wish to point out that, although simplifications of the above expression are possible in restricted cases, in general calculation times increase rapidly with the number of partial waves (l_a, l_c, and l_d) which must be included for the three distorted waves. This is partially owing to the somewhat complicated multiple summation which must be carried out, and partially simply to increases in computing times for individual vector coupling coefficients involving large angular momenta (especially since the variables kq are not restricted to small values). As a result, calculations for higher energies can become prohibitively time consuming and many groups have been obliged to introduce additional approximations such as a Wentzel-Kramers-Brillouin (WKB) representation for the distorted waves.[15]

When spin-orbit terms are included, problems become even more severe. Details of the expressions which must be evaluated have been given by Jackson.[16] Since each distorted wave becomes a matrix in spin space, additional spin summations and vector coupling coefficients enter, thus leading to a rather formidable calculation.

In order to simplify the calculation and to achieve acceptable computing times, we have chosen to eliminate essentially all angular momentum algebra from the calculation. Thus, we simply evaluate integrals of the form given in Eq. (1) directly rather than expressions similar to that given in Eq. (2). At first sight, this appears to be a poor decision since we must now evaluate a complicated three-dimensional integral rather than a linear combination of one-dimensional integrals. However, in practice, impressive savings in computing time result. For example, for an $L=0$ $(p,2p)$ calculation involving 30 partial waves for each particle, the direct integration method is roughly 80 times faster than a conventional evaluation of Eq. (2). For $L=2$, the savings increase to almost a factor of 110. Even greater savings are achieved for calculations necessitating more partial waves. Finally, on introducing spin-orbit terms, the direct integration calculation is slowed only by a factor of 3 to 4 so that computing times are still much superior to spin independent calculations employing conventional angular momentum algebra.

Basically, our new method owes its success to the fact that remarkably few Gaussian integration points are needed for convergence. Typically, 15—20 points in each of r, θ, and ϕ suffice (i.e., a few thousand points total), irrespective of the number of partial waves. For a calculation with 50 partial waves, this is to be contrasted with several tens of thousands of radial integrals entering the summation appearing in Eq. (2), and an identical number of angular coefficients which are involved even *after* the summations over k, q, and λ_d are completed.

The small number of integration points needed is, of course, a numerical matter to be addressed in individual cases. However, a number of observations may be illuminating. Firstly, the complexity of Eq. (2) arises from explicit use of partial wave expansions which isolate pieces of each distorted wave which vary rapidly with angle. In contrast, the product of all three distorted waves may vary rather slowly. An extreme example is a knockout reaction

at zero recoil momentum, in which, if distortion effects are negligible, the product

$$H(\vec{r})=\chi_c^{(-)*}\chi_d^{(-)*}\chi_a^{(+)}$$

is actually constant. Thus, for an $L=0$ transition the integrand would be independent of angle and the only radial variation is due to $\phi_{LA}(\vec{r})$. Secondly, even if $H(\vec{r})$ does exhibit significant variation with $\vec{r}$, rather coarse integration methods may suffice in view of the relatively slow variation of $\phi_{LA}(\vec{r})$. For example, if 50 partial waves are used in each channel, $H(\vec{r})$ contains multipoles up to $l\sim 150$. However, only the $l=L$ term contributes to the integral. Thus, an angular integration method which rather crudely averages the rapidly varying higher multipoles of $H(\vec{r})$ can yield good results provided the low multipoles close to $l=L$ are accurately treated. Similar comments apply to the radial integration provided we are not dealing with unusually high momentum components.

B. Formulation

In order to proceed we must recast the formalism given by Jackson[16] in a form suitable for our proposed direction three-dimensional integration method of calculation. Since the distorted waves take especially simple forms when expressed in a system in which the $\hat{z}$ axis is parallel to the direction of propagation, we first introduce three separate sets of axes Q_a, Q_c, and Q_d as shown in Fig. 1. Quantities expressed with respect to these axes are identified as unprimed, primed, and double primed, respectively. The directions of propagation of particles a, c, and d are thus the $\hat{z}$, $\hat{z}'$, and $\hat{z}''$ axes, respectively. The outgoing particle directions are characterized by angles θ_c, θ_d, and β as indicated in the figure, thus permitting calculations for noncoplanar geometries. A fourth set of axes Q_p, employing a triple-primed notation, permits simple treatment of polarized projectiles. For the present calculations the polarization axis $\hat{z}'''$ has been restricted to the orientation shown, normal to the plane defined by particles a and c. Generalization to other orientations is straightforward.

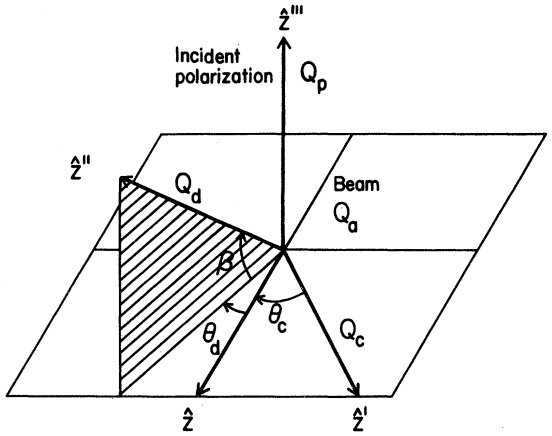

FIG. 1. Relative orientation of axes used in calculations. The direction of propagation of particles a, c, and d are parallel to $\hat{z}$, $\hat{z}'$, and $\hat{z}''$, respectively. The incident particle polarization axis is $\hat{z}'''$.

Assuming for simplicity particles a through d have spin $\frac{1}{2}$ and denoting spin projections by ρ_i, the transition amplitude in Q_a can be written

$$\langle\rho_c\rho_d\,|\,T\,|\,\rho_aJM\rangle=\sum_{\rho_c'\rho_d''}D^{(1/2)*}_{\rho_c'\rho_c}(R_{ca})D^{(1/2)*}_{\rho_d''\rho_d}(R_{da})\langle\rho_c'\rho_d''\,|\,T\,|\,\rho_aJM\rangle\ , \tag{3}$$

where the $D^{1/2}_{mn}(R)$ are rotation matrices, R_{ca} and R_{da} are rotations into Q_a of Q_c and Q_d, respectively, and J,M are the total angular momentum quantum numbers of particle b. Using the orthonormality of the D functions, we can write the differential cross section for an unpolarized incident beam as

$$\sigma_{BA}=\frac{2\pi}{\hbar v}\omega_BC^2S\sum_{\substack{\rho_a\rho_c'\rho_d''\\JM}}\frac{|\langle\rho_c'\rho_d''\,|\,T\,|\,\rho_aJM\rangle\,|^2}{(2J+1)(2S_a+1)}\ , \tag{4}$$

where $S_a=\frac{1}{2}$ is the spin of particle a. The additional quantities are v the incident velocity, ω_B the phase space factor, and C^2S the spectroscopic factor. For an incident polarized beam we can construct the analyzing power in terms of the cross section for a spin projection ρ_a''' in Q_p where

$$\sigma_{BA}(\rho_a''')=\frac{2\pi}{\hbar v}\omega_BC^2S\sum_{\substack{\rho_c'\rho_d''\\JM}}\frac{\left|\sum_{\rho_a}\langle\rho_c'\rho_d''\,|\,T\,|\,\rho_aJM\rangle D^{1/2}_{\rho_a\rho_a'''}(R_{ap})\right|^2}{(2J+1)} \tag{5}$$

and R_{ap} rotates Q_a into Q_p.

To proceed we write

$$T=\Omega_c^{(-)}\Omega_d^{(-)}t\Omega_a^{(+)}\ , \tag{6}$$

where

$$\Omega^{(\pm)}|\rho\rangle=\sum_{\sigma}\chi^{(\pm)}_{\sigma\rho}(\vec{\mathrm{r}})\,|\,\sigma\rangle \tag{7}$$

and

$$|JM\rangle=\sum_{\Lambda\sigma_b}(L\Lambda S_b\sigma_b\,|\,JM)\phi_{L\Lambda}(\vec{\mathrm{r}})\,|\,\sigma_b\rangle\ . \tag{8}$$

Hence,

$$\langle\rho_c'\rho_d''\,|\,T\,|\,\rho_a JM\rangle=\sum_{\substack{\sigma_a\sigma_c'\sigma_d''\\ \Lambda\sigma_b}}(2L+1)^{1/2}(L\Lambda S_b\sigma_b\,|\,JM)T^{L\Lambda}_{\substack{\sigma_a\sigma_c'\sigma_d''\\ \rho_a\rho_c'\rho_d''}}\langle\sigma_c'\sigma_d''\,|\,t\,|\,\sigma_a\sigma_b\rangle\ , \tag{9}$$

where we have made the usual factorization approximation in separating the matrix elements of the two-body transition operator t outside the distorted wave integral. The quantity $T^{L\Lambda}$ is defined by

$$T^{L\Lambda}_{\substack{\sigma_a\sigma_c'\sigma_d''\\ \rho_a\rho_c'\rho_d''}}=(2L+1)^{-1/2}\int\chi^{(-)*}_{\sigma_c'\rho_c'}(\vec{\mathrm{r}}')\chi^{(-)*}_{\sigma_d''\rho_d''}(\vec{\mathrm{r}}'')\phi_{L\Lambda}(\vec{\mathrm{r}})\chi^{(+)}_{\sigma_a\rho_a}(\gamma\vec{\mathrm{r}})d\vec{\mathrm{r}}\ , \tag{10}$$

which is the generalization of Eq. (1).

The distorted waves appearing in the integrand are obtained from the radial wave functions U_{lj} in the usual fashion. Specifically,

$$\chi^{(+)}_{\sigma_a\rho_a}(\vec{\mathrm{k}}_a,\vec{\mathrm{r}})=\frac{4\pi}{kr}\sum_{lj\lambda\lambda' m}(l\lambda\tfrac{1}{2}\rho_a\,|\,jm)(l\lambda'\tfrac{1}{2}\sigma_a\,|\,jm)i^l U_{lj}(k_a,r)Y^*_{l\lambda}(\hat{k}_a)Y_{l\lambda'}(\hat{r})\ . \tag{11}$$

For our choice of axes $\hat{k}_a\equiv\hat{z}$ so that use of explicit expressions for the vector coupling coefficients yields

$$\chi^{(+)}_{\sigma_a\rho_a}(\vec{\mathrm{k}}_a,\vec{\mathrm{r}})=(k_a r)^{-1}\sum_l i^l[(l+1)U_{lj_+}(k_a,r)+lU_{lj_-}(k_a,r)]d^l_{00}(\theta) \tag{12a}$$

for $\sigma_a=\rho_a$, and

$$\chi^{(+)}_{\sigma_a\rho_a}(\vec{\mathrm{k}}_a,\vec{\mathrm{r}})=\pm(k_a r)^{-1}\sum_l i^l[l(l+1)]^{1/2}[U_{lj_+}(k_a,r)-U_{lj_-}(k_a,r)]d^l_{10}(\theta)e^{\pm i\phi}\ , \tag{12b}$$

For $\sigma_a=-\rho_a=\pm\frac{1}{2}$, where $j_\pm=l\pm\frac{1}{2}$. Applying the usual time reversal relation ships yields

$$\chi^{(-)*}_{\sigma_c'\rho_c'}(\vec{\mathrm{k}}_c,\vec{\mathrm{r}}')=(k_c r)^{-1}\sum_{l'} i^{-l'}[(l'+1)U_{l'j'_+}(k_c,r)+l'U_{l'j'_-}(k_c,r)]d^{l'}_{00}(\theta') \tag{13a}$$

and

$$\chi^{(-)*}_{\sigma_c'\rho_c'}(\vec{\mathrm{k}}_c,\vec{\mathrm{r}}')=\pm(k_c r)^{-1}\sum_{l'} i^{-l'}[l'(l'+1)]^{1/2}[U_{l'j'_+}(k_c,r)-U_{l'j'_-}(k_c,r)]d^{l'}_{10}(\theta')e^{\mp i\phi'}\ , \tag{13b}$$

for $\sigma_c'=\rho_c'$ and $\sigma_c'=-\rho_c'$, respectively. Similar expressions in terms of r, θ'', and ϕ'' are obtained for particle d. Finally, $\phi_{L\Lambda}(\vec{\mathrm{r}})=R(r)Y_{L\Lambda}(\hat{r})$ can be written

$$\phi_{L\Lambda}(\vec{\mathrm{r}})=R(r)\left[\frac{2L+1}{4\pi}\right]^{1/2}d^L_{\Lambda 0}(\theta)e^{i\Lambda\phi}\ . \tag{14}$$

Thus, the integration (10) can be carried out using Eqs. (12)—(14) in conjunction with simple expressions for (θ',ϕ') and (θ'',ϕ'') in terms of (θ,ϕ) to evaluate the integrand at each Gaussian mesh point in r,θ,ϕ.

In order to complete the calculation it is necessary to substitute for the two-body t matrix in Eq. (9). This is related to a t matrix in which all spin projections are referred to Q_a by

$$\langle \sigma_c' \sigma_d'' \mid t \mid \sigma_a \sigma_b \rangle = \sum_{\sigma_c \sigma_d} D^{1/2*}_{\sigma_c \sigma_c'}(R_{ac}) D^{1/2*}_{\sigma_d \sigma_d''}(R_{ad}) \langle \sigma_c \sigma_d \mid t \mid \sigma_a \sigma_b \rangle \ , \tag{15}$$

and the latter t matrix can be related to the usual amplitudes expressed in a channel spin representation.[17] Our final expression for spin projection ρ_a''' is thus

$$\sigma_{BA}(\rho_a''') = \frac{2\pi}{\hbar v} \omega_B C^2 S \sum_{\substack{\rho_c' \rho_d'' \\ JM}} \frac{1}{2J+1} \left| \sum_{\substack{\rho_a \sigma_a \sigma_c \sigma_c' \\ \sigma_d \sigma_d'' \sigma_b \Lambda}} (2L+1)^{1/2} (L \Lambda S_b \sigma_b \mid JM) \right.$$

$$\times D^{1/2}_{\rho_a \rho_a'''}(R_{ap}) D^{1/2*}_{\sigma_c \sigma_c'}(R_{ac}) D^{1/2*}_{\sigma_d \sigma_d''}(R_{ad})$$

$$\left. \times T^{L\Lambda}_{\substack{\sigma_a \sigma_c' \sigma_d'' \\ \rho_a \rho_c' \rho_d''}} \langle \sigma_c \sigma_d \mid t \mid \sigma_a \sigma_b \rangle \right|^2 , \tag{16}$$

where the amplitude $T^{L\Lambda}$ is defined by Eqs. (10)—(14). It is this expression which is evaluated in the computer code THREEDEE used for the calculations described in Sec. III. Since we are dealing with spin $\frac{1}{2}$ particles, simple analytic expressions are, of course, available for the D matrices.[18]

III. RESULTS

Calculations for the $(p,2p)$ and (p,pn) reactions have been carried out using the global optical model parameters of Nadasen *et al.*[19] which were obtained from fits to proton elastic scattering data taken at incident energies of 80 to 180 MeV. The wave function for the bound nucleon was generated in the usual fashion as an eigenfunction of a Woods-Saxon well adjusted to reproduce the empirical separation energy. The corresponding geometrical parameters are listed in Table I. The two-body t matrix,

$$\langle \sigma_c \sigma_d \mid t \mid \sigma_a \sigma_b \rangle \ ,$$

was obtained by interpolating available on-shell nucleon-nucleon phase shifts.[20] Despite the use of a factorized expression for the overall amplitude, this scattering is, more properly, half off the energy shell[21] owing to the binding of the struck nucleon in the target. For the present, we ignore this complication and, in common with most of the earlier work, approximate the corresponding t matrix with the on-shell amplitude at either the initial or final relative energies. These choices are referred to as initial/final energy prescriptions (IEP/FEP), respectively. In the calculations which follow, in the absence of specific statements to the contrary, it may be assumed that we have utilized the FEP and that IEP results are not qualitatively different.

TABLE I. Bound nucleon potential parameters. The notation is identical with that used in Ref. 1.

Reaction	r_0 (fm)	a (fm)	V_{SO} (MeV)
^{40}Ca$(p,2p)^{39}$K	1.3	0.6	12.0
^{40}Ca$(p,pn)^{39}$Ca	1.3	0.6	12.0
^{208}Pb$(p,2p)^{207}$Tl	1.25	0.63	5.0

In Ref. 14 we presented calculations and data[22] at an incident energy of 150 MeV for ^{40}Ca$(p,2p)^{39}$K (2.52 MeV) which is a $2s_{1/2}$ $L=0$ transition. Calculations for a quasifree angular distribution or "factorization test," in which the angular variation of the differential cross section is measured at kinematic conditions such that the residual nucleus recoil momentum, P_B, is zero, were found to be rather little changed on introducing spin orbit distortions (aside from an overall renormalization of $\sim 10\%$). The corresponding polarization analyzing powers are shown in Fig. 2(a). In the absence of spin-orbit terms the analyzing power is predicted to be identical to the free p-p analyzing power.[14] Thus, the calculations are presented as a function of the effective p-p c.m. scattering angle. The angular range is restricted at forward angles by the requirement that both detected particles have energies in excess of 20 MeV. This is a typical constraint, both from experimental considerations and to minimize possible contributions from sequential processes. It is seen that there are significant quantitative differences between the spin orbit (SO) and no spin orbit (NSO) analyzing powers, although there are no major qualitative effects. Similarly, for the corresponding differential cross sections shown in Fig. 2(b), inclusion of spin-orbit distortions does not lead to major qualitative changes. However, the peak cross section is reduced

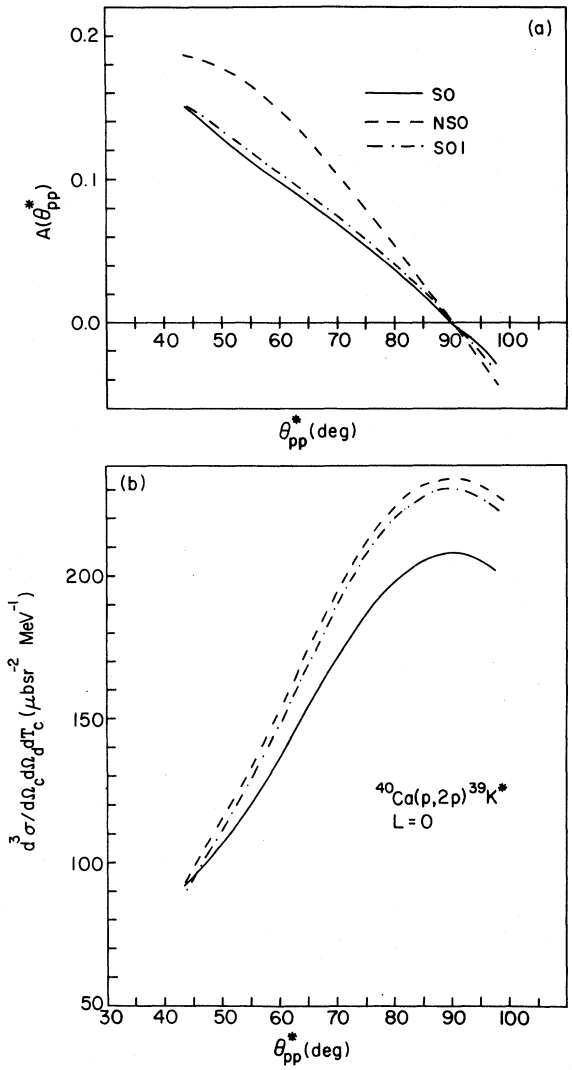

FIG. 2. Calculations for a quasifree angular distribution for ^{40}Ca$(p,2p)^{39}$K (2.52 MeV) at an incident energy of 150 MeV as a function of the effective $p+p$ scattering angle. The kinematics is chosen such that the residual nucleus is at rest. The notation SO, NSO, SO1 is defined in the text. (a) Polarization analyzing powers; (b) differential cross sections.

by $\sim 12\%$ leading to a more modest decrease with decreasing values of $\theta_{pp}^{\text{c.m.}}$ than in the NSO calculation. Also shown in Fig. 2 are calculations (denoted SO1) in which spin-orbit distortions are included only for the incident proton. In the case of the analyzing powers, these lie close to the SO results so that the emitted proton spin-orbit terms have little influence. This is presumably a consequence of the fact that the polarization of these particles is not measured so that a sum over both spin projections is involved.[14,24] Since the ratio of SO to NSO analyzing powers is $\sim 70\%$, independent of angle, one can thus interpret the results as arising from an average depolarization of the incident beam of $\sim 30\%$. This is significantly larger than the WKB approximation estimate (of $\sim 5\%$) obtained[23] for ^{40}Ca at 320 MeV. In contrasts to the behavior of the analyzing powers, the SO1 differential cross sections lie close to the NSO results. Thus, it is the spin-orbit terms for the emitted protons which are largely responsible for the reduction in cross section between the NSO and SO predictions. Inspection of the calculations reveals that this is not a complicated effect involving interference between several of the spin dependent distorted wave amplitudes defined in Eq. (10). Rather, it is due almost entirely to a reduction in the single complex amplitude involving no spin flip (i.e., $\rho_i = \sigma_i$ for all three particles) which dominates the

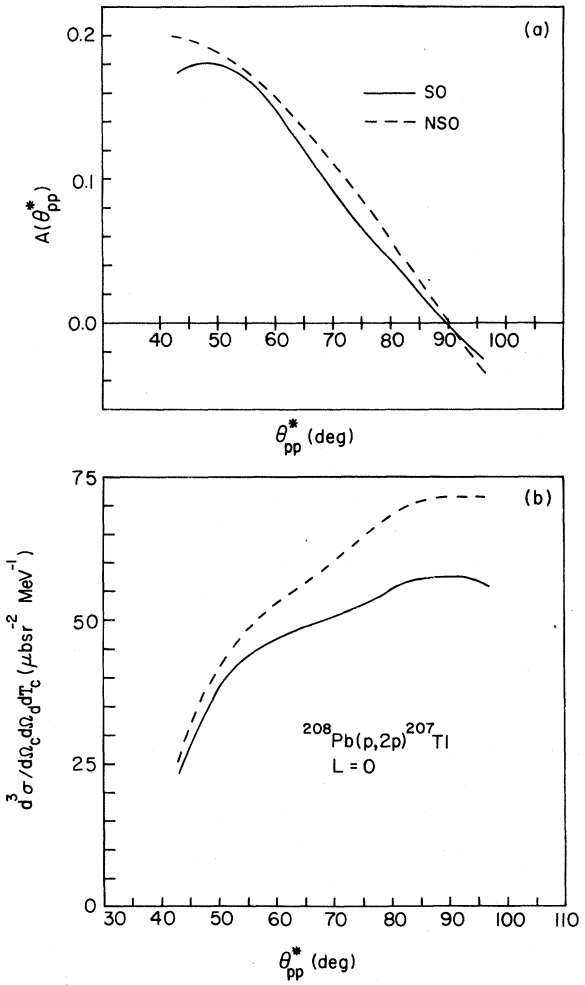

FIG. 3. Calculations for a quasifree angular distribution for ^{208}Pb$(p,2p)^{207}$Tl (g.s.) at an incident energy of 150 MeV as a function of the effective $p+p$ scattering angle. The kinematics is chosen such that the residual nucleus is at rest. (a) Polarization analyzing powers; (b) differential cross section.

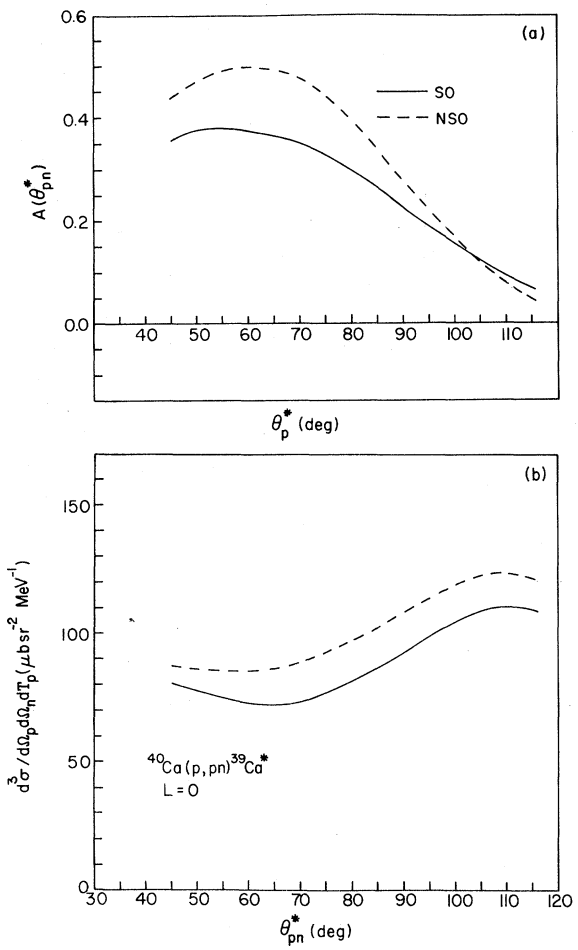

FIG. 4. Calculations for a quasifree angular distribution for ^{40}Ca(p,pn)^{39}Ca (2.47 MeV) at an incident energy of 150 MeV as a function of the effective $p+n$ scattering angle. The kinematics is chosen such that the residual nucleus is at rest. (a) Polarization analyzing powers; (b) differential cross sections.

calculation of the differential cross section.

Somewhat larger effects might be expected for more massive nuclei. This follows since the spin-orbit potential strength is proportional to the projectile orbital angular momentum. Thus, for ^{208}Pb, for example, the spin-orbit terms should be roughly 70% stronger for the presumably important surface partial waves than for ^{40}Ca. Results for ^{208}Pb($p,2p$)^{207}Tl (g.s.) at 150 MeV are shown in Fig. 3. This is an $L=0$ ($3s_{1/2}$) transition so that, again, the NSO analyzing powers are identical to the free p-p values. In fact, we see that, contrary to the preceding argument, the effects of including spin-orbit terms are significantly smaller than for ^{40}Ca although the relative change in differential cross section is somewhat greater. That arguments based on dominance by a few surface partial waves are poor is consistent with the observation that the DWIA transition amplitude is $\sim$0.2 of the corresponding plane wave calculation. Thus, distortion effects are not especially severe [at least in comparison with reactions such as (α,2α), where the corresponding ratio of amplitudes can exceed 1/100].

In Fig. 4, results are shown for ^{40}Ca(p,pn)^{39}Ca (2.47 MeV) which is the analog $L=0$ transition to the ($p,2p$) case shown in Fig. 2. The comparison is of interest since the spin structure for $p+n$ scattering is somewhat different from the $p+p$ case. Specifically, singlet-odd and triplet-even terms can now enter. While the singlet-odd force is weak, the triplet-even force, which is responsible for the binding of the deuteron, is strong and is dominated by the tensor force. (For example, in the Hamada-Johnston potential[25] the triplet-even tensor term is roughly twice the triplet-even central term at 1.4 fm.) In view of this major difference in the two-body t-matrix spin structure, we speculate that the effects of the optical potential spin-orbit terms may differ qualitatively between analog (p,pn) and ($p,2p$) transitions. We see from Fig. 4 that this is not the case. While the NSO (p,pn) analyzing powers are somewhat larger than for ($p,2p$) (being again identical to the free two-body values) the effect of the spin-orbit terms is to reduce the analyzing powers in much the same fashion as for ($p,2p$). For the differential cross sections there is essentially a constant reduction in magnitude of $\sim$11% due to the addition of the spin-orbit terms. Thus, the angular variation is somewhat flatter than that shown for ($p,2p$) in Fig. 2(b). This change does not arise from differences in the spin structure of the amplitudes. Rather, it is a consequence of differences in kinematics owing to the differing neutron and proton separation energies in ^{40}Ca. As a result of slightly lower emitted particle energies for the (p,pn) reaction, distortion effects are somewhat greater at large values of θ^* than for the ($p,2p$) case. While the predictions shown are not inconsistent with experiment,[14,30] sensitivity to the parametrization of the nucleon optical potential can be expected and should be evaluated in any careful analysis of these reactions.

In the preceding calculations of $L=0$ quasifree angular distributions, kinematic conditions were chosen so that at all angles the residual nucleus was left at rest. It follows from plane wave impulse approximation arguments that this choice minimizes sensitivity to the struck nucleon momentum wave function and that much of the resultant angular variation arises from a changing nucleon-nucleon t matrix. An alternative procedure is to select kinematic conditions in which the situation is reversed so that, aside from phase space and distortion effects, cross section variations predominantly re-

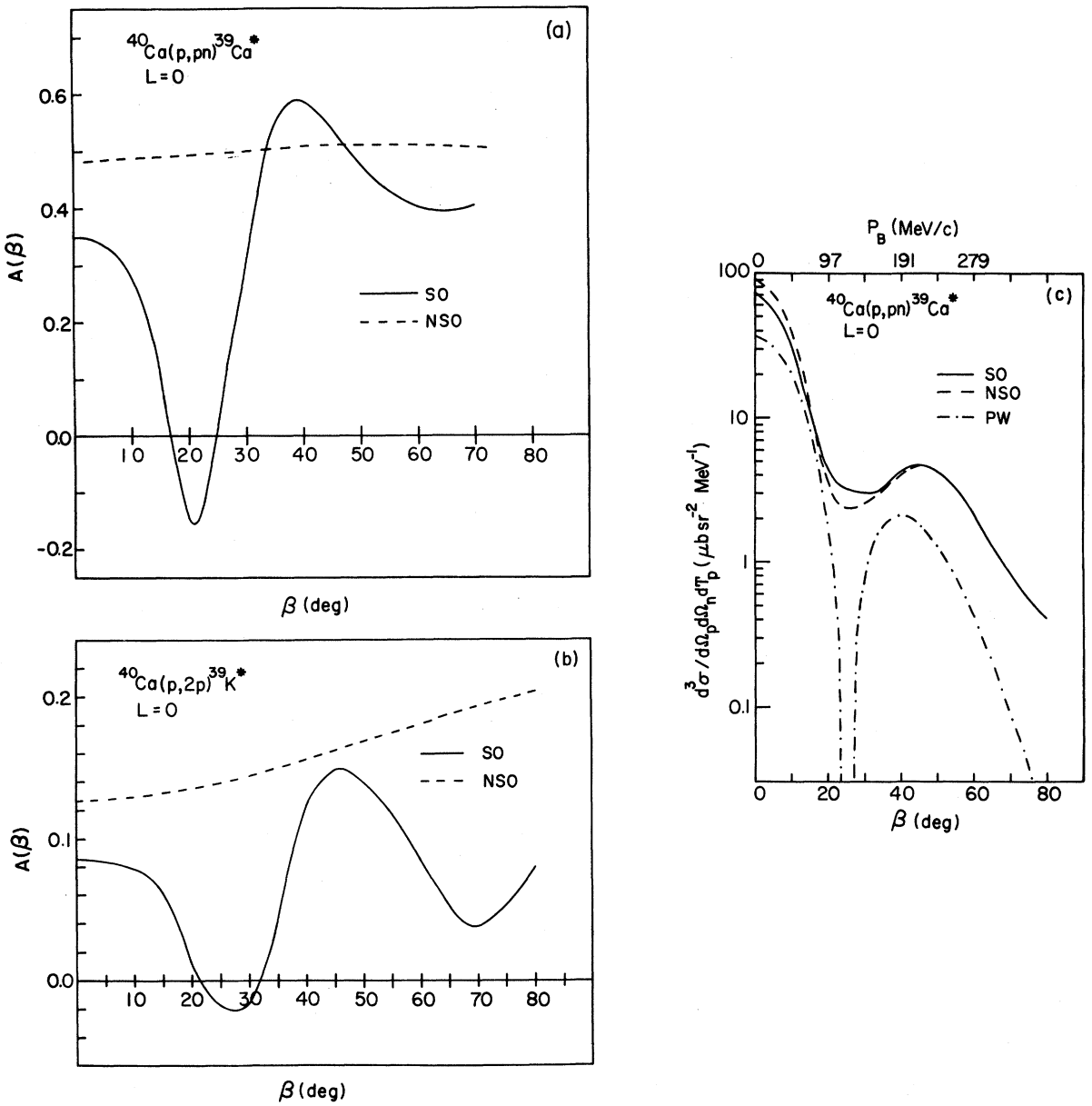

FIG. 5. Calculations for $L=0$ nucleon knockout from ^{40}Ca at an incident energy of 150 MeV using a noncoplanar geometry. Following the notation of Fig. 1, $\theta_c=30°$, $\theta_d=48.7°$, and the detected energy of proton c is $T_c=90.38$ MeV. (a) Polarization analyzing power for ^{40}Ca$(p,pn)^{39}$Ca (2.47 MeV); (b) polarization analyzing power for ^{40}Ca$(p,2p)^{39}$K (2.52 MeV); (c) differential cross section for ^{40}Ca$(p,pn)^{39}$Ca (2.47 MeV). The curve labeled PW is the square of the struck neutron momentum wave function in arbitrary units plotted as a function of P_B, the recoil momentum of the residual nucleus.

flect the momentum dependence of the struck nucleon wave function. Possibilities include measuring angular distributions in a noncoplanar geometry, coplanar symmetric angular distributions, and so-called energy sharing distributions.[31]

Measurements using a noncoplanar geometry have been shown, for $(p,p\alpha)$ reactions, to lead to enhanced sensitivity to the cluster-core momentum wave function.[26,27] Some results have also been reported for nucleon knockout reactions.[28,29] As an example, in Fig. 5(a), polarization analyzing powers for ^{40}Ca$(p,pn)^{39}$Ca (2.47 MeV) are shown as a function of β, the angle of noncoplanarity defined in Fig. 1. For $\beta=0$ the detectors and incident beam are coplanar while the detected particle angles θ_p/θ_n and detected proton energy T_p correspond to a zero recoil momentum point or "quasifree" condition. For the other points, T_p and θ_p are held fixed while

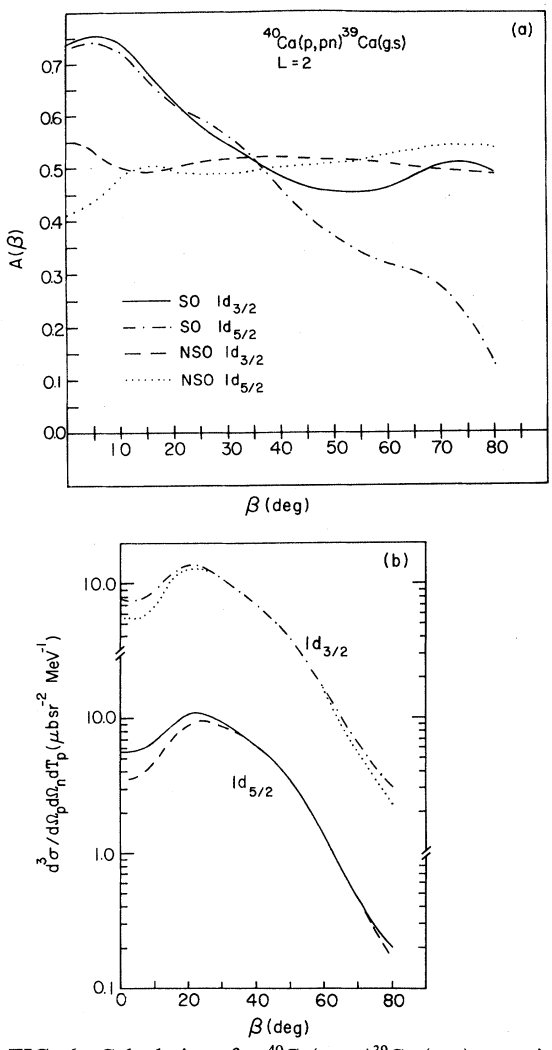

FIG. 6. Calculations for ^{40}Ca(p,pn)^{39}Ca (g.s.) at an incident energy of 150 MeV in a noncoplanar geometry. In the notation of Fig. 1, $\theta_c=30°$, $\theta_d=48.7°$, and $T_c=90.38$ MeV. Both $1d_{3/2}$ and $1d_{5/2}$ transitions are shown. (a) Polarization analyzing powers; (b) differential cross section.

the neutron detector is rotated in a plane normal to the original scattering plane through an angle β. For the angular range shown, recoil momenta range from zero to $\sim$350 MeV/c. Unlike the previous cases discussed, there are large differences between the SO and NSO analyzing powers. Specifically, near $\beta=30°$ the SO result swings rapidly from positive to negative values and back again. In contrast, the NSO result varies slowly over the entire angular range studied. In Fig. 5(b) we see that similar behavior is exhibited by the analyzing powers for the analog ($p,2p$) transition, although the overall magnitudes are smaller due to the differing nucleon-nucleon amplitudes. Referring to Fig. 5(c), in which the cross section is shown for the (p,pn) case, it is clear that the rapid change in analyzing power can be correlated with a minimum in the unpolarized cross section which arises from a node in the neutron momentum wave function at $\sim$120 MeV/c. Similar relationships have been found in studies of polarization effects in other reactions. Thus, precise measurements of both cross section and analyzing power should serve to constrain both the calculation of spin-orbit effects and the treatment of the bound state wave function.

Referring again to Fig. 5(c), we see that the introduction of spin-orbit distortions has fairly modest effects on the differential cross section. Specifically, the cross section at the $\beta=0$ maximum is reduced by $\sim$17%, while the minimum at $\sim$120 MeV/c is somewhat shallower in the SO calculation than in the NSO case. This latter effect is not surprising since, in the plane wave limit, the $\sim$120 MeV/c point coincides with a node in the $2s_{1/2}$ wave function, and has zero cross section. Thus, the nonzero cross section predicted at this point is solely a consequence of distortion effects. Specifically, it is the result of refraction permitting contributions from nonzero parts of the neutron momentum distribution. Since, in the SO calculation distortion effects differ in the $j=l\pm\frac{1}{2}$ partial waves, some greater degree of smearing with respect to the NSO calculation seems likely.

In Fig. 6, polarization analyzing powers and differential cross sections are presented for ^{40}Ca(p,pn)^{39}Ca (g.s.) at 150 MeV. We again consider a noncoplanar geometry with a detected proton energy and with proton and neutron angles θ_c/θ_d chosen to be the same as for the preceding calculations. For the ground state transition, a neutron is ejected from the $1d_{3/2}$ shell. However, for comparison purposes, calculations assuming $1d_{5/2}$ are also shown. From Fig. 6(b) it is clear that, in common with the preceding $L=0$ calculations and with the $L=2$ calculations of Ref. 14 for a coplanar geometry, the differential cross sections are not drastically changed on introducing spin-orbit distortions. However, for the rather large analyzing powers shown in Fig. 6(a), this is not the case. While the SO analyzing powers do not exhibit the rapid angular variation noted for $L=0$ in Fig. 5, they do differ significantly from the NSO predictions. In particular, while the NSO analyzing powers exhibit rather modest differences between $1d_{3/2}$ and $1d_{5/2}$ transitions (for the particular kinematics considered), the corresponding SO calculations diverge markedly for angles beyond $\beta\approx40°$.

Somewhat more common than measurements of noncoplanar angular distributions are measurements of "energy sharing distributions" in which the detected particle angles are fixed and cross sections

are extracted as a function of detected energy. In this type of measurement there is, in principle, some variation of the nucleon-nucleon t matrix. However, the behavior of the cross section is normally dominated by the changing struck nucleon momentum wave function.

Results of ^{40}Ca$(p,2p)^{39}$K at 148.2 MeV have already been presented[14] for both $L=0$ and $L=2$ transitions. For the differential cross section, effects due to inclusion of spin-orbit distortions were quite small aside from the renormalization of the $L=0$ cross section previously noted. It should be emphasized that there was no corresponding change in the $L=2$ cross section, so that the introduction of spin-orbit distortions produced a change in *relative* spectroscopic factors.

Calculations for ^{208}Pb$(p,2p)^{207}$Tl at 150 MeV incident energy are shown in Figs. 7 and 8 for $L=0$, $3s_{1/2}$ and $L=2$, $2d_{3/2}$ proton knockout, respectively. For the $L=0$ cross sections shown in Fig. 7(a), we see that the peak cross section in the SO calculation is reduced by $\sim 20\%$ with respect to the NSO result. In addition, the minimum at ~ 43 MeV in the NSO curve, which results from a node in the $3s_{1/2}$ momentum wave function, is shifted to lower energies and becomes shallower in the SO calculation. For the $L=0$ analyzing power calculations in Fig. 7(b) the NSO result is not shown. It is negligibly small at all detected energies considered since the corresponding $p+p$ scattering angle is always close to 90° c.m. In contrast, the SO result is large and changes sign close to the energy of the minimum in the corresponding differential cross section. In Fig. 8(a) the cross section for the $L=2$, $2d_{3/2}$ transition to the 0.351 MeV excited level of ^{207}Tl does not show large changes on introducing spin-orbit distortions. However, for the polarization analyzing

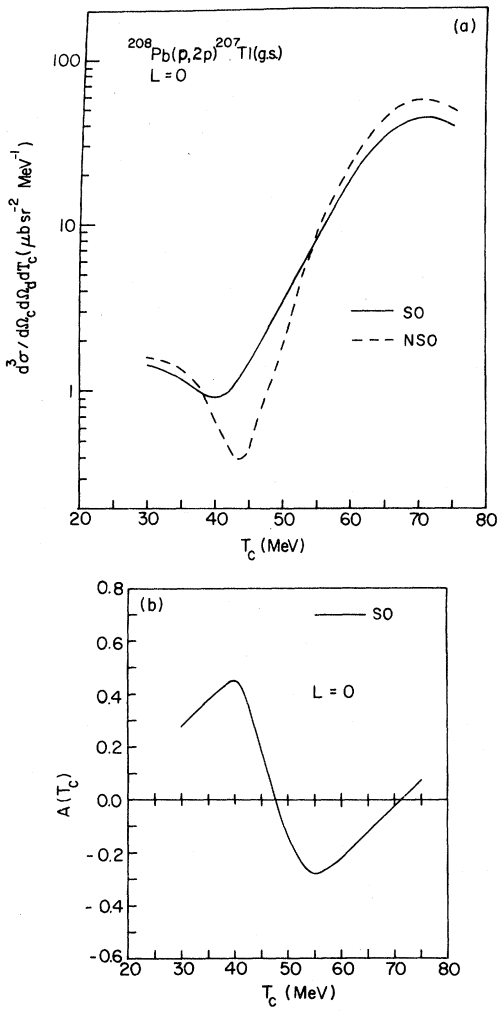

FIG. 7. Calculations of the $L=0$ $(3s_{1/2})$ energy sharing distribution for ^{208}Pb$(p,2p)^{207}$Tl (g.s.) at an incident energy of 150 MeV, $\theta_c=\theta_d=45.12°$. (a) Differential cross section; (b) polarization analyzing power.

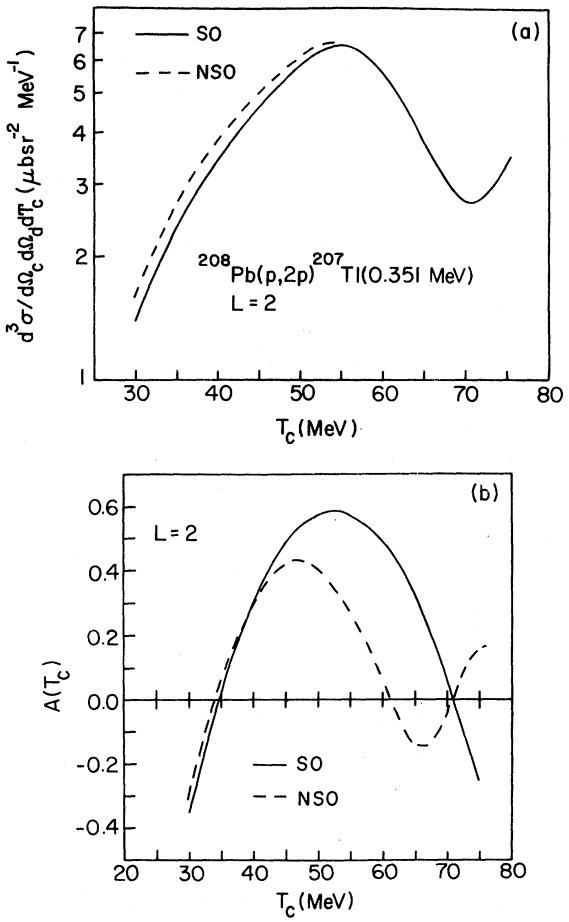

FIG. 8. Calculations of the $L=2$ $(2d_{3/2})$ energy sharing distribution for ^{208}Pb$(p,2p)^{207}$Tl (g.s.) at an incident energy of 150 MeV, $\theta_c=\theta_d=45.12°$. (a) Differential cross section; (b) polarization analyzing power.

powers in Fig. 8(b) there are again quite large effects. Specifically, as we approach equal emitted proton energies at ~70.8 MeV (which is a point of symmetry since we are considering equal and opposite emitted proton angles) the small negative excursion which is predicted in the NSO calculations is entirely eliminated in the SO curve. That the spin-orbit terms are relatively important in this region is consistent with the fact that, in the plane wave limit, the cross section is zero at this point. However, in contrast to the behavior noted at nodes in $L=0$ wave functions, in the present example the spin-orbit terms serve to eliminate a more complicated NSO distortion effect, perhaps as a result of greater averaging.

In measurements of coplanar symmetric angular distributions[31] (CSAD) particles are detected in a plane at equal angles on either side of the beam with equal energies. Consequently, for $(p,2p)$ the polarization analyzing power must be identically zero owing to the left-right symmetry of the experiment. Analyses[32] of CSAD differential cross sections for ^{4}He$(p,2p)^3$H at 250 to 500 MeV incident energy have shown that, though negligible at angles corresponding to recoil momenta below about 250 MeV/c, the spin-orbit terms do change the predictions significantly at higher momenta and, in fact, improve agreement with experiment.

Predicted differential cross sections for ^{208}Pb$(p,2p)^{207}$Tl (g.s.) at 150 MeV incident energy are shown in Fig. 9 for a CSAD measurement. On the basis of plane wave arguments a CSAD prediction can be expected to show much the same dependence on residual nucleus recoil momentum as the corresponding energy sharing measurement. Thus, a curve qualitatively similar to that shown in Fig. 7(a) was anticipated. From Fig. 9 we see that this is not the case. In fact, distortion effects have generated a double peaked structure more reminiscent of an $L\neq 0$ transition. In view of this rather special distortion effect it is no surprise that the inclusion of spin-orbit terms in the optical potentials has a major effect on the relative heights of the two peaks. In Fig. 10 CSAD predictions are shown for ^{40}Ca$(p,2p)^{39}$K (2.52 MeV) at an incident energy of 150 MeV. For this $L=0$, $2s_{1/2}$ transition the NSO distribution shows the anticipated shape with a single peak at low recoil momenta. Thus, the special distortion effect encountered for the preceding case is presumably absent and we would anticipate smaller differences between SO and NSO predictions, which indeed proves to be the case.

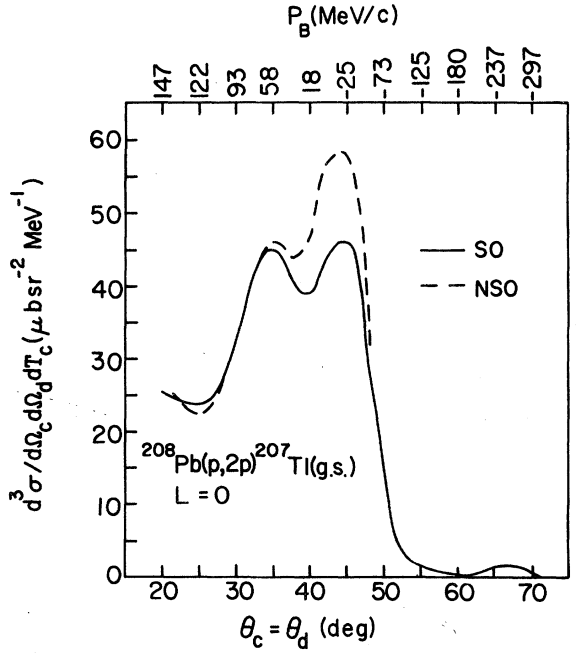

FIG. 9. Calculations of the coplanar symmetric $(T_c=T_d,\theta_c=\theta_d)$ angular distribution of the differential cross section for ^{208}Pb$(p,2p)^{207}$Tl (g.s.) $L=0$, $3s_{1/2}$ at an incident energy of 150 MeV.

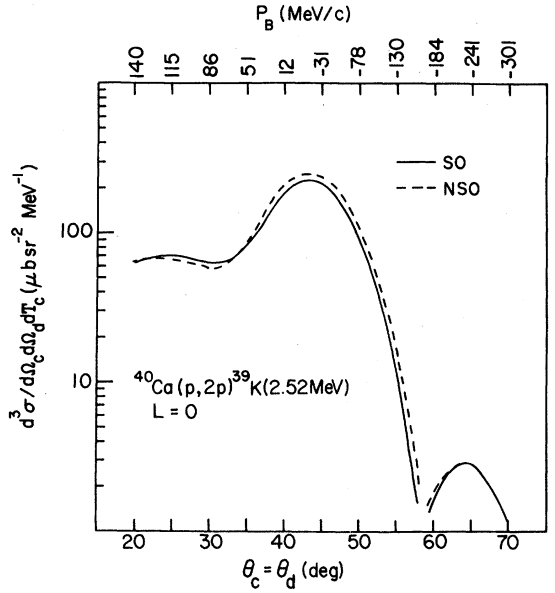

FIG. 10. Calculations of the coplanar symmetric $(T_c=T_d,\theta_c=\theta_d)$ angular distribution of the differential cross section for ^{40}Ca$(p,2p)^{39}$K (2.52 MeV) $L=0$, $2s_{1/2}$ at an incident energy of 150 MeV.

IV. SUMMARY AND CONCLUSIONS

A new procedure for DWIA calculations of quasi-free knockout reactions has been described in which the explicit calculation of angular momentum coupling coefficients is replaced by a three-dimensional

numerical integration. The procedure is simple to generalize to include spin-orbit terms in the distorting potentials and the resultant computer calculation is considerably faster (and cheaper) than conventional NSO calculations employing Racah algebra.

Sample calculations for 150 MeV $(p,2p)$ and (p,pn) reactions were presented. The incident energy was selected partially because of the availability of good optical potentials for this energy region and partially because of proposed experiments at this energy. In general, the effects of including spin-orbit distorting potentials are not negligible. For differential cross section predictions there were no major qualitative changes aside from a CSAD prediction for ^{208}Pb. However, errors of 10% to 20% in relative spectroscopic factors are to be expected for analyses employing NSO calculations.

For polarization analyzing powers, relatively modest differences between SO and NSO predictions for "factorization tests" or quasifree angular distribution measurements were found. However, for measurements involving a range of residual nucleus recoil momenta (and hence expected to be determined largely by the changing struck nucleon momentum wave function), major differences between SO and NSO calculations were noted. Most notable was a rapid change in the polarization analyzing power correlated with a node in the momentum wave function for $L=0$. This proved to be a general feature of both $(p,2p)$ and (p,pn) calculations for both energy sharing and noncoplanar angular distribution data. If it can be found experimentally, this should prove useful in constraining the assumed struck nucleon wave function and in testing the accuracy of the spin dependence of the scattering waves generated by the optical potential chosen for subsequent DWIA analyses.

For $L>0$ transitions much of the j dependence of the polarization analyzing power is known to arise from polarization of the struck nucleon due to spin independent (NSO) spatial localization effects.[2] In $L=2$ calculations for an energy sharing distribution the major features of the NSO predictions remained in the SO results although there were changes in detail. On the other hand, calculations for a noncoplanar angular distribution showed greater differences between NSO and SO predictions with the latter, suggesting somewhat enhanced j dependence at large angles.

Finally, it should be noted that, while it does in general appear to be important to include spin-orbit distortions in DWIA analyses of $(p,2p)$ and (p,pn) reactions, other generalizations from the small number of specific calculations presented here are probably unwise. Clearly, it is now highly desirable to turn to the question of off-shell effects on the nucleon-nucleon t matrix in order to further refine the analysis.

ACKNOWLEDGMENTS

We are indebted to Dr. Peter Kitching for encouragement and assistance in the early phases of this work. The calculations presented herein were carried out using the UNIVAC computers of the Computer Science Center of the University of Maryland. Provision of computing time by the Center is gratefully acknowledged. This work was supported in part by the National Science Foundation.

[1]P. G. Roos *et al.*, Phys. Rev. Lett. 40, 1439 (1978).
[2]C. A. Miller, in *Proceedings of the Ninth International Conference on the Few-Body Problem,* edited by M. J. Moravcsik and F. S. Levin (University of Oregon, Eugene, 1980), Vol. I; in *Common Problems in Low- and Medium-Energy Nuclear Physics,* edited by B. Castel, B. Coulard, and F. C. Khanna (Plenum, New York, 1979), p. 513.
[3]W. J. McDonald, Nucl. Phys. A335, 463 (1980).
[4]N. S. Chant, in *Clustering Aspects of Nuclear Structure and Nuclear Reactions (Winnipeg, 1978),* Proceedings of the Third International Conference on Clustering Aspects of Nuclear Structure and Nuclear Reactions, AIP Conf. Proc. No. 47, edited by W. T. H. van Oers, J. P. Sveene, J. S. C. McKee, and W. R. Falk (AIP, New York, 1978), p. 415.
[5]P. G. Roos *et al.*, Phys. Rev. C 15, 69 (1977).
[6]T. A. Carey, P. G. Roos, N. S. Chant, A. Nadasen, and H. L. Chen, Phys. Rev. C 23, 576 (1981).
[7]N. S. Chant and P. G. Roos, Phys. Rev. C 15, 57 (1977).
[8]D. F. Jackson and T. Berggren, Nucl. Phys. 62, 353 (1965).
[9]E. F. Redish, Phys. Rev. Lett. 31, 617 (1973).
[10]N. Austern, Phys. Rev. Lett. 41, 1696 (1978).
[11]D. F. Jackson, Phys. Scr. 25, 514 (1982).
[12]K. L. Lim and I. E. McCarthy, Nucl. Phys. 88, 433 (1966).
[13]R. D. Koshel, Nucl. Phys. A260, 401 (1976).
[14]N. S. Chant, P. Kitching, P. G. Roos, and L. Antonuk, Phys. Rev. Lett. 43, 495 (1979).
[15]Th. A. J. Maris, in *Nuclear and Particle Physics at Intermediate Energies,* edited by J. B. Warren (Plenum, New York, 1976), p. 425.
[16]D. F. Jackson, Nucl. Phys. A257, 221 (1976).
[17]M. H. MacGregor, R. A. Arndt, and R. M. Wright, Phys. Rev. 182, 1714 (1969).
[18]D. M. Brink and G. R. Satchler, *Angular Momentum* (Oxford University Press, Oxford, 1962).
[19]A. Nadasen *et al.*, Phys. Rev. C 23, 1023 (1981).
[20]C. A. Miller, private communication.

[21]E. F. Redish, G. J. Stephenson, Jr., and G. M. Lerner, Phys. Rev. C 2, 1665 (1970).
[22]P. G. Roos *et al.*, Phys. Rev. Lett. 40, 1939 (1978).
[23]G. Jacob, Th. A. Maris, C. Schneider, and M. R. Teodoro, Nucl. Phys. A257, 517 (1976).
[24]C. Schneider, Nucl. Phys. A300, 313 (1978).
[25]T. Hamada and I. D. Johnston, Nucl. Phys. 34, 38a (1962).
[26]A. Nadasen *et al.*, Phys. Rev. C 22, 1394 (1980).
[27]A. Nadasen *et al.*, Phys. Rev. C 23, 2353 (1981).
[28]T. Yuasa and E. Hourany, Nucl. Phys. A103, 577 (1967).
[29]E. Hourany *et al.*, Nucl. Phys. A162, 624 (1971).
[30]J. Watson, private communication.
[31]P. G. Roos, in *Momentum Wave Functions—1976 (Indiana University),* Proceedings of the Workshop/Seminar on Momentum Wave Function Determination in Atomic, Molecular, and Nuclear Systems, AIP Conf. Proc. No. 36, edited by D. W. Devins (AIP, New York, 1977), p. 32.
[32]W. T. H. van Oers *et al.*, Phys. Rev. C 25, 390 (1982); M. B. Epstein *et al.*, Phys. Rev. Lett. 44, 20 (1980).